Behavioral/Systems/Cognitive

The Synaptic Representation of Sound Source Location in Auditory Cortex

Paul Chadderton,[1,2] John P. Agapiou,[1,2] David McAlpine,[1,2] and Troy W. Margrie[1,3]

[1]Department of Neuroscience, Physiology, and Pharmacology, University College London, London WC1E 6BT, United Kingdom, [2]UCL Ear Institute, London WC1X 8EE, United Kingdom, and [3]Division of Neurophysiology, The National Institute for Medical Research, London NW7 1AA, United Kingdom

A key function of the auditory system is to provide reliable information about the location of sound sources. Here, we describe how sound location is represented by synaptic input arriving onto pyramidal cells within auditory cortex by combining free-field acoustic stimulation in the frontal azimuthal plane with *in vivo* whole-cell recordings. We found that subthreshold activity was panoramic in that EPSPs could be evoked from all locations in all cells. Regardless of the sound location that evoked the largest EPSP, we observed a slowing in the EPSP slope along the contralateral–ipsilateral plane that was reflected in a temporal sequence of peak EPSP times. Contralateral sounds evoked EPSPs with earlier peak times and consequently generated action potential firing with shorter latencies than ipsilateral sounds. Thus, whereas spiking probability reflected the region of space evoking the largest EPSP, across the population, synaptic inputs enforced a gradient of spike latency and precision along the horizontal axis. Therefore, within auditory cortex and regardless of preferred location, the time window of synaptic integration reflects sound source location and ensures that spatial acoustic information is represented by relative timings of pyramidal cell output.

Introduction

Neural activity within auditory cortex is necessary for sound localization (Heffner and Masterton, 1975; Jenkins and Masterton, 1982; Thompson and Cortez, 1983; Jenkins and Merzenich, 1984; Kavanagh and Kelly, 1987; Heffner and Heffner, 1990; Malhotra and Lomber, 2007), but mechanisms by which acoustic space is represented remain to be determined. For example, no evidence has been found for a spatiotopic map within core regions of auditory cortex (Middlebrooks and Pettigrew, 1981; Imig et al., 1990; Rajan et al., 1990a,b). Instead, tonotopic organizations are found in primary auditory cortex (A1) and neighboring core areas such as anterior (AAF) and ventral (VAF) auditory fields (Kalatsky et al., 2005; Polley et al., 2007). It therefore seems that sound location must be represented by other means (Wise and Irvine, 1985; Brugge et al., 1996; Stecker and Middlebrooks, 2003; Stecker et al., 2005). The main inputs to A1, AAF and VAF are thalamocortical pathways projecting from the ventral medial geniculate body (vMGB) to neurons in layers 2–4 (Winer, 1992; Cruikshank et al., 2002; Read et al., 2002). Neurons within these layers receive thalamic and local cortical projections (Kaur et al., 2004; Barbour and Callaway, 2008), although the synaptic properties of these inputs have not been studied in the context of sound localization.

In A1 neurons, extracellular recordings have been used to investigate the encoding of sound location in the spike rates (Middlebrooks and Pettigrew, 1981; Wise and Irvine, 1985; Imig et al., 1990; Rajan et al., 1990a,b; Brugge et al., 1996; Stecker and Middlebrooks, 2003; Mrsic-Flogel et al., 2005; Stecker et al., 2005; Werner-Reiss and Groh, 2008). Such neurons are tuned to preferred locations predominately within the contralateral hemifield (Middlebrooks and Pettigrew, 1981; Wise and Irvine, 1985; Imig et al., 1990; Rajan et al., 1990a; Middlebrooks and Green, 1991; Brugge et al., 1996; Mickey and Middlebrooks, 2003; Stecker and Middlebrooks, 2003; Mrsic-Flogel et al., 2005; Stecker et al., 2005). Sound location also modulates spike timing (Brugge et al., 1996; Eggermont, 1998; Middlebrooks et al., 1998; Furukawa and Middlebrooks, 2002; Mickey and Middlebrooks, 2003; Stecker et al., 2003; Mrsic-Flogel et al., 2005): contralateral sounds typically evoke the earliest action potentials, while spike latency increases across the contralateral–ipsilateral axis (Eggermont, 1998). It remains unclear whether the measures of spike latency and rate/probability might differentially encode spatial information (Eggermont and Mossop, 1998; Stecker and Middlebrooks, 2003).

To understand how spatially tuned output is generated in auditory cortex, it is critical to study the properties of the underlying synaptic inputs. Understanding the organization of subthreshold input will shed light on the degree of pre-processing of spatial information and emergent features of sound source representation in auditory cortex. Here, we have used *in vivo* whole-cell recordings in the auditory cortex of the rat to explore the synaptic basis of sound localization in a free-field environment. We show that the amplitude and temporal profile of evoked synaptic input are modulated by sound location

Received May 1, 2009; revised Aug. 22, 2009; accepted Sept. 5, 2009.

This work was supported by grants from the Wellcome Trust (T.W.M., D.M.), the Human Frontier Science Program (T.W.M.), and the Medical Research Council (D.M., T.W.M.), a European Union Marie Curie Fellowship (P.C.), and a Wellcome Trust four-year PhD studentship (J.P.A.). We thank Michael Pecka and Ede Rancz for comments.

This article is freely available online through the *J Neurosci* Open Choice option.

Correspondence should be addressed to Troy W. Margrie, Division of Neurophysiology, The National Institute for Medical Research, The Ridgeway, Mill Hill, London NW7 1AA, UK. E-mail: troy.margrie@nimr.mrc.ac.uk.

J. P. Agapiou's present address: Center for Physics and Biology, Rockefeller University, 1230 York Avenue, New York, NY 10021.

DOI:10.1523/JNEUROSCI.2061-09.2009

 0270-6474/09/2914127-09$15.00/0

independently, enforcing a temporal representation of auditory space in the output of pyramidal cells.

Materials and Methods

Surgical procedures and preparation. The care and experimental manipulation of animals was performed in accordance with institutional and United Kingdom Home Office guidelines. Twenty- to 24-d-old Sprague Dawley rats were anesthetized with urethane (1.4 g/kg) via intraperitoneal injection. When animals were areflexive, they were secured in a custom-built stereotaxic plate using hollow cheek bars. A craniotomy was performed over auditory cortex (3.5 mm posterior, 7 mm lateral of bregma) (Paxinos and Watson, 2004), and the dura was removed under high magnification (20×). In all but one instance, the craniotomy was made over the right hemisphere. The animal was then moved in the stereotaxic plate to the center of a large anechoic chamber, in which it was secured to the top of an aluminum pole 1 m above the floor. Low-resistance patch pipettes (4–6 MΩ) were fabricated from filamented borosilicate glass capillaries (outer diameter, 1.5 mm and inner diameter, 0.86 mm; Harvard Apparatus), using a Narishige PC10 vertical puller. A low-magnification dissection scope, mounted behind the animal, was used to manually position patch pipettes orthogonal to, and just above, the pial surface. The experimenter moved to an adjoining room, having sealed the anechoic chamber, and guided the patch pipette (under high pressure) onto the surface of the brain using a remote-controlled automated micromanipulator (SM-4; Luigs and Neumann).

Electrophysiological recordings. An Axoclamp 2B amplifier (Molecular Devices) was used to search for, and record from, neurons *in vivo*. Initially, contact between the patch pipette and the brain surface was indicated via a square current pulse on an oscilloscope in response to square voltage injections. At this point, the depth was noted, subsequently allowing the depth of recorded neurons beneath the pia to be determined. Blind whole-cell recordings were then performed in voltage-recording mode, as described previously (Margrie et al., 2002). The internal solution contained the following (in mM): 133 K-methanesulphonate, 7 KCl, 10 HEPES, 2 Mg-ATP, 2 Na_2-ATP, 0.5 Na_2-GTP, and 0.05 EGTA. Biocytin (0.5%) was also added to the solution.

Neuronal classification. We investigated the spatial receptive fields (SRFs) of pyramidal cells only. Pyramidal cells were identified on the basis of input resistance, action potential (AP) waveform (in particular, the absence of fast afterhyperpolarization) (Margrie et al., 2003), and subsequent morphological reconstruction (Horikawa and Armstrong, 1988) (Fig. 1*a*) (supplemental Fig. S1*a*, available at www.jneurosci.org as supplemental material). Neuronal input resistance was calculated from steady-state voltage deflections during 400 ms step current injection (−200 pA). Pyramidal cells had lower input resistances than fast-spiking interneurons and slower repolarizations after AP firing (time-to-peak hyperpolarization) (Table 1). Neurons included in this study were all located ≤700 μm from the pial surface (supplemental Fig. S1*b*, available at www.jneurosci.org as supplemental material). Pyramidal cells were included in the analysis of synaptic and spiking SRFs if stimuli evoked APs from at least one tested location. One cell was excluded on the basis that all tested azimuths evoked APs with probability ~1, and thus it did not exhibit spatial tuning of its output per se.

Whole-cell recordings were targeted to A1 on the basis of stereotaxic coordinates and vascular structure (Paxinos and Watson, 2004; Kalatsky et al., 2005), and a reliable short-latency excitatory response to contralateral white-noise stimulation (evoked EPSP onset, 17.8 ± 0.3 ms; $n = 38$) (Polley et al., 2007) (supplemental Fig S1*c*, available at www.jneurosci.org as supplemental material). However, the absence of pronounced differences in cytoarchitecture (Rutkowski et al., 2003) and the similarity between many physiological parameters (Polley et al., 2007) across core auditory fields meant that we could not eliminate the possibility that some recordings were made from auditory fields directly adjacent to A1 (e.g., VAF and AAF).

Free-field auditory stimulation. During recordings, rats were situated in the center of a sound-attenuating anechoic chamber (IAC), and stimuli were presented from an array of 15 calibrated speakers (KFC-1066; Kenwood), positioned at a distance of 1 m from the animal's head in the frontal azimuthal plane (range, ±78.75°; spacing, 11.25°). All stimuli were noise bursts [50 ms, 65 dB sound pressure level (SPL) measured at the head], digitally generated at a sampling rate of 50 kHz by filtering Gaussian-distributed white noise.

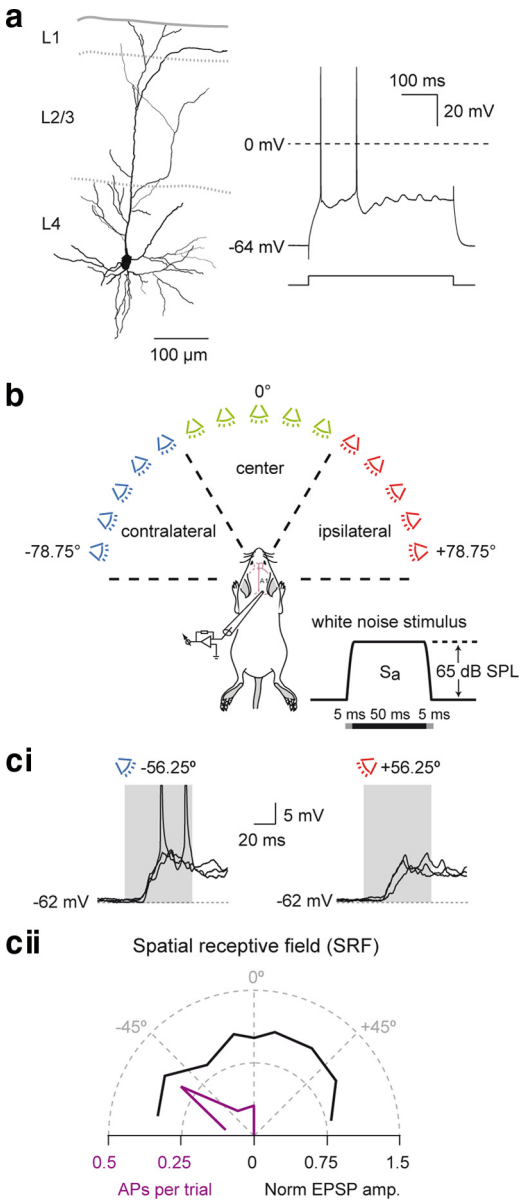

Figure 1. Spiking versus synaptic SRFs in layer 2–4 pyramidal cells. ***a***, Morphological reconstruction (left) and spiking profile (right) for a single layer 4 pyramidal cell. ***b***, SRFs were probed using identical cosine-ramped (5 ms) white-noise stimuli (65 dB SPL, 50 ms), presented from individual speakers at a frequency of 0.2 Hz. For classification purposes, the 15 locations could be divided into three groups: contralateral (−78.75° to −33.75°; blue), central (−22.5° to +22.5°; green), and ipsilateral (+33.75° to +78.75°; red). ***ci***, Responses evoked in a layer 4 pyramidal cell by sounds from two different locations (3 consecutive trials, overlaid). Top left, Sounds presented from a contralateral location evoked EPSPs and action potentials (action potentials are truncated). Top right, Sounds presented from an ipsilateral location evoked subthreshold EPSPs only. ***cii***, Synaptic (black) and spiking (purple) SRFs for the same cell.

The stimulus for each speaker was digitally generated and filtered on one of 15 dedicated real-time processors (RP2; Tucker-Davis Technologies), which could be triggered synchronously (via the zBus interface; Tucker-Davis Technologies). Stimulus presentation was controlled via a personal computer running the Brainware program (Tucker-Davis Technologies). Presentation and recording were synchronized using a transistor–transistor logic pulse mediated by another real-time processor (RP2.1; Tucker-Davis Technologies). Noise was high-pass filtered at 0.1 kHz and low-pass filtered at 18 kHz (second-order Butterworth filters)

Table 1. Characteristics of pyramidal cells and fast-spiking interneuron recordings

Intrinsic feature	Pyramidal cells ($n = 38$)	Fast-spiking cells ($n = 8$)	p value
V_m (mV)	-57.8 ± 1.1	-61.6 ± 4.1	0.21
R_{input} (MΩ)	39.6 ± 2.1	81.3 ± 9.7	2.2×10^{-8}
t_m	9.2 ± 0.5	6.4 ± 0.6	0.026
AP half-width (ms)	1.10 ± 0.05	0.60 ± 0.08	2.5×10^{-4}
AHP peak amplitude (mV)	-7.9 ± 0.5	-6.1 ± 1.0	0.094
Time of AHP peak (ms)	54.5 ± 4.5	8.2 ± 4.9	2.2×10^{-5}
Spontaneous firing rate (Hz)	0.54 ± 0.08	1.33 ± 0.73	0.87*
Depth from surface (μm)	479 ± 12	480 ± 42	0.98

Statistical differences were calculated using Student's unpaired t test or *Mann–Whitney U test. AHP, Afterhyperpolarization.

and gated with ramped cosine windows (5 ms to 90% of maximum). The token of noise used to generate the stimulus was changed for each set of presentations. Before presentation, stimuli were inverse filtered to compensate for the frequency response of the speaker from which they would be presented. This ensured that any difference between the neural responses to different sources was a consequence of azimuthal position and not an artifact of differences in the frequency response of individual speakers. The desired stimulus was filtered by a 512-tap finite impulse response filter that closely approximated the inverse transfer function of each speaker. The transfer function for each speaker was measured using Golay-pair stimuli (Zhou et al., 1992), and the output of each speaker was recorded using a high quality ½ inch microphone (type 4134; Brüel and Kjær), preamplifier (type 2669; Brüel and Kjær), and measurement amplifier (type 2610; Brüel and Kjær). The transfer function was recorded from the anechoic chamber with the microphone positioned where the animal's head would be.

For whole-cell recordings, it was necessary to introduce several objects into the chamber: the platform/heating pad on which the animal rested, cheek restraints, a dissecting microscope and the microelectrode manipulator. To avoid acoustic shadowing, the microscope and manipulator were positioned as far behind and away from the animal's head as possible. The metal cheek bars were custom made, with minimal profile, and positioned as low as possible. Thus, although stimuli were identical at source, differences in the position of equipment relative to different sources were likely to result in extraneous spectral differences at the ears as a consequence of reflections.

Spatial receptive field mapping. SRFs were mapped for individual cells using the average voltage recordings of nonspiking evoked responses to static stimuli (10 or more sweeps per location). Typically 9 or 15 locations were tested across the range of ±78.75°. EPSP onset was defined as the time at which membrane potential reached 5% of peak amplitude. EPSP rising slope corresponded to the 10–90% rate of rise of the mean EPSP waveform. "Preferred" and "least-preferred" locations were defined as the single speaker locations that evoked the largest and smallest amplitude EPSPs, respectively. Cells were assigned to one of three classes representing subregions of azimuth on the basis of the mean response to all of the tested locations within that region, i.e., cells were defined as "contralateral" if the evoked EPSP was largest on average for sampled locations between −78.75° and −33.75°, rather than between −22.5° to +22.5° ("central"), or +33.75° to +78.75° ("ipsilateral") (Fig. 1*b*). Spiking responses to static stimuli were defined by the occurrence of APs within 100 ms of stimulus onset (in the absence of direct current injection).

Data acquisition and analysis. Data were low-pass filtered at 3 kHz and acquired at 20 kHz via an ITC-18 interface (InstruTECH) and an Apple G5 PowerPC using Axograph X software (Axograph Scientific). Data were analyzed offline using Axograph X and Igor Pro (Wavemetrics). All data are presented as mean ± SEM unless otherwise stated.

SRF bandwidth was classified as the azimuth encompassing all the sound locations that evoked EPSP amplitudes or spike probabilities ≥25, 50, and 75% of the magnitude of the response evoked at the preferred location (values denoted, respectively, as BW_{25}, BW_{50}, and BW_{75}).

Results

Panoramic synaptic potentials ensure broad spatial receptive fields in pyramidal cells

Whole-cell recordings were made from pyramidal neurons in the superficial layers (2–4) of auditory cortex in urethane-anesthetized rats (Fig. 1*a*) (Margrie et al., 2002). To investigate the relationship between excitatory synaptic input and spatially tuned pyramidal cell output, we systematically varied the location of a 50 ms burst of white noise across the frontal hemifield (65 dB SPL; 11.25° increments from −78.25° to +78.25°; $n = 38$ pyramidal cells tested with at least 3 sound locations) (Fig. 1*b*). Sounds evoked AP firing in a fraction of recordings (14 of 38 cells), typically only one AP per trial (DeWeese et al., 2003; Stecker et al., 2003; Ulanovsky et al., 2004; Hromádka et al., 2008). As a result, location-dependent modulation of AP firing was reflected as a change in spike probability rather than as a modulation of ongoing firing rates. Commonly, spiking responses were only evoked by sounds emanating from a small fraction of tested locations (Fig. 1*c*). In contrast, evoked EPSPs were observed in all cells and at all locations tested (overall peak EPSP amplitude, 5.21 ± 0.57 mV; range, 1.06–9.99 mV; $n = 22$ of 38 cells in which all speaker locations were tested). Thus, synaptic SRFs were panoramic, extending fully across the tested range of azimuth (Fig. 1*c*).

In cases in which we could directly compare the entire synaptic and spiking SRFs ($n = 6$ cells), the sound location eliciting the strongest response was the same for the EPSP amplitude and spiking probability. A perfect correlation existed between the locations evoking the peak subthreshold and peak spiking responses for all six neurons ($r = 1$, $p < 0.02$, Spearman's rank correlation coefficient). However, spike probability exhibited a greater fractional reduction than EPSP amplitude across azimuth (strongest to weakest sound locations: $p < 0.01$, $n = 6$, Wilcoxon's signed rank test; spike probability: 60.3 ± 8.4 to 2.6 ± 6.2%; normalized EPSP amplitude: 1.33 ± 0.09 to 0.74 ± 0.04 at the same locations) (Fig. 2*a*). Therefore, spiking SRFs declined in magnitude more steeply with distance from preferred azimuths (Fig. 2*b*). This sharpening of the spatial tuning of pyramidal cell output was reflected in the significantly narrower bandwidth of spiking versus synaptic SRFs (50% bandwidth: 45 ± 17° vs 124 ± 10° for spiking and synaptic azimuthal bandwidth, respectively; $p < 0.01$, $n = 6$ for spiking and $n = 22$ for synaptic SRFs, Mann–Whitney U test) (Fig. 2*c*). Thus, as for frequency tuning (Wehr and Zador, 2003; Kaur et al., 2004), a broadly tuned subthreshold input underlies spatial processing in auditory cortical pyramidal cells.

Preferred locations are distributed across azimuth with a contralateral bias

Because sounds always evoked EPSPs but not APs, preferred locations were subsequently defined using the synaptic SRF: the preferred location for a given cell being the sound source azimuth that evoked the largest amplitude EPSP (Fig. 3*a*). Across the dataset, we found preferred locations to be distributed across azimuth. To make comparisons between neurons with different spatial preferences, we assigned neurons on the basis of their preferred location to one of three groups: contralateral, central, and ipsilateral (with respect to the recorded cerebral hemisphere) (Fig. 1*b*). We found that the majority of neurons preferred sounds from contralateral locations (20 of 38 cells) (Fig. 3*b*), consistent with the spatial preference of APs (8 of 14 cells in this study) (Middlebrooks and Pettigrew, 1981; Wise and Irvine, 1985; Imig et al., 1990; Rajan et al., 1990a; Middlebrooks and

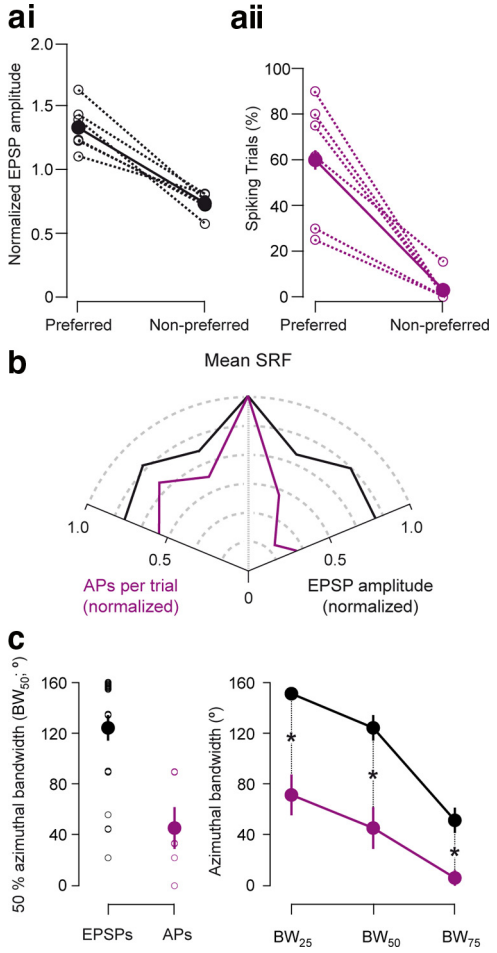

Figure 2. Narrow bandwidth of spiking SRFs compared with underlying synaptic input. ***ai***, Decline in evoked EPSP amplitude (normalized to mean amplitude across all locations) from strongest to weakest stimulus azimuths in cells in which subthreshold and suprathreshold responses were recorded. ***aii***, Decline in spiking probability from strongest to weakest stimulus azimuths in the same cells. ***b***, Peak-aligned average synaptic and spiking SRFs for six cells in which both were recorded. ***c***, Left, 50% bandwidth (BW_{50}) of synaptic and spiking SRFs for individual cells. Right, Synaptic and spiking receptive field bandwidth at 25% (BW_{25}), 50%, and 75% response thresholds (BW_{75}). Spiking SRFs were significantly narrower (*$p < 0.01$, paired *t* test, $n = 22$).

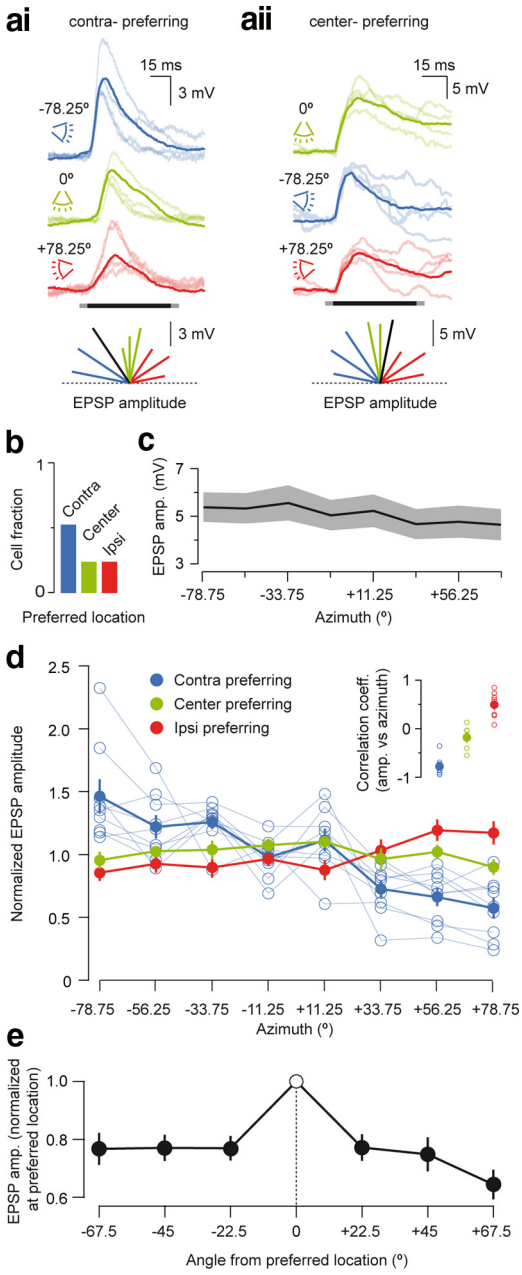

Figure 3. Cell-specific synaptic SRFs are broadly tuned. ***ai***, Top, Individual and average (bold) EPSPs from a contralateral-preferring neuron evoked by sounds presented from contralateral (blue), central (green), and ipsilateral (red) locations. Bar indicates when stimulus is on (black) and ramped onset/offset (gray). Bottom, SRF for the same cell. Angles correspond to speaker azimuths, and black line indicates maximum. ***aii***, Top, Individual and average (bold) EPSPs from a center-preferring neuron evoked by sounds presented from contralateral (blue), central (green), and ipsilateral (red) locations. Bar indicates when stimulus is on (black) and ramped onset/offset (gray). Bottom, SRF for the same cell. Angles correspond to speaker azimuths, and black line indicates maximum. ***b***, Distribution of preferred location across azimuth ($n = 38$ cells). ***c***, Pooled average (black line) and SEM (gray area) of EPSP amplitude ($n = 22$ cells). ***d***, Mean synaptic SRFs (filled circles) for contralateral-preferring (blue), central-preferring (green), and ipsilateral-preferring (red) neurons. Individual contralateral-preferring synaptic SRFs are also shown (blue, open circles). Inset, Correlation between azimuth and EPSP amplitude for contralateral-preferring (blue), central-preferring (green), and ipsilateral-preferring neurons. ***e***, Change in EPSP amplitude with angular deviation from preferred location ($n = 22$ cells).

Green, 1991; Brugge et al., 1996; Stecker and Middlebrooks, 2003; Mrsic-Flogel et al., 2005; Stecker et al., 2005). However, despite an overall preference for contralateral sounds, the overall difference in mean EPSP amplitude for the population was rather small between the most contralateral and most ipsilateral locations (Fig. 3*c*, Table 2), and there was no overall relationship between sound location and EPSP amplitude (EPSP amplitude vs azimuth: $p = 0.09$, Friedman's test, $n = 22$). This was attributable to a substantial fraction of cells with central or ipsilateral preferred locations. The relationship between azimuth and EPSP amplitude differed between the three cell groups (Fig. 3*d*): in the case of ipsilateral-preferring cells, the change in EPSP amplitude with azimuth mirrored that of contralateral-preferring cells (i.e., positive rather than negative correlation coefficients) (Fig. 3*d*, inset). Nevertheless, for any given cell and regardless of preferred location, evoked EPSP amplitudes decreased by a similar magnitude with increasing angular deviation in either direction from the preferred location (Fig. 3*e*). On average, an angular deviation of 45° reduced EPSP amplitude by 28.1 ± 0.1% ($n = 10$) and 29.1 ± 0.1% ($n = 9$) in contralateral- and ipsilateral-preferring cells, respectively ($p > 0.5$, unpaired *t* test). Thus, within a single cerebral hemisphere, contralateral space is over-represented, but there are neurons that individually respond most strongly to all locations across frontal horizontal space.

Table 2. Properties of evoked synaptic and spiking responses with respect to azimuth in auditory cortical pyramidal cells

Property of evoked response	Contralateral (−78.75°)	Center (0°)	Ipsilateral (−78.75°)	*p* value
EPSP amplitude (mV)	5.38 ± 0.62	5.03 ± 0.65	4.64 ± 0.65	0.21
EPSP rising slope (Vs)	1.02 ± 0.19	0.75 ± 0.13	0.48 ± 0.09	6.2×10^{-7}
EPSP onset latency (ms)	17.7 ± 0.4	18.1 ± 0.5	18.5 ± 0.3	4.0×10^{-7}
EPSP peak latency (ms)	26.9 ± 1.2	30.3 ± 1.6	35.5 ± 1.7	8.0×10^{-4}
AP probability (APs/trial)	0.42 ± 0.09	0.38 ± 0.08	0.31 ± 0.07	0.52
AP latency (ms)	26.6 ± 3.2	33.4 ± 3.7	35.0 ± 2.3	0.082*
SD of AP latency (ms)	4.1 ± 1.5	7.2 ± 1.6	10.0 ± 2.0	0.047*

Statistical differences were calculated using Friedman's or *Kruskal–Wallis test ($n = 22$ for EPSP properties, $n = 14$ for AP properties).

The rising slope of synaptic potentials independently reports sound source location

Although the majority of cells preferred contralateral sound sources, there was sufficient heterogeneity across the population such that no significant relationship between sound location and EPSP amplitude was observed. However, we found a striking relationship between sound location and EPSP rising slope (Fig. 4*a*). Across the population, EPSP rising slope decreased systematically with azimuth, such that contralateral sounds consistently evoked EPSPs with faster rising slopes than those evoked by ipsilateral sounds (10–90% EPSP rising slope vs azimuth: $p < 0.001$, Friedman's test, $n = 22$) (Fig. 4*b*, Table 2). EPSP rising slope was strongly and significantly correlated with azimuth ($r = -0.51 \pm 0.09$, $p < 0.01$, sign test, $n = 22$), whereas EPSP amplitude showed no overall bias ($r = -0.18 \pm 0.14$, $p = 0.08$, sign test, $n = 22$). Accordingly and in contrast to EPSP amplitude, we observed a striking asymmetry in the change in EPSP rising slope with increasing angular deviation from the preferred location. Only sounds emanating from regions of space more ipsilateral than the preferred location evoked progressively slower rising synaptic responses (Fig. 4*c*). Thus, the fastest rising EPSPs were always evoked from contralateral sound sources regardless of the preferred location of the cells.

Contralateral-preferring cells represented the largest fraction of our dataset, and, in these cells, a strong correlation between EPSP amplitude and rising slope was observed across locations (Fig. 4*d*). However, this correlation was significantly weaker for cells whose preferred locations lay within central and ipsilateral sectors because these cells still typically exhibited their fastest rising EPSPs in response to contralateral sounds ($p < 0.02$, Kruskal–Wallis test, $n = 22$) (Fig. 4*b*,*d*). Consequently, across the population, the azimuths that evoked the largest EPSPs and those that evoked the steepest-rising EPSPs differed significantly ($p < 0.01$, $n = 22$, paired *t* test). Therefore, the relationship between sound location and EPSP rising slope in auditory cortical pyramidal cells is fixed and independent of the SRF of a cell.

Rapid EPSP rising slopes reduce latency and variability of action potentials evoked by contralateral sounds

Although EPSP onset latency also varied significantly with sound location ($p < 0.001$, Friedman's test, $n = 22$) (Fig. 5*a*), the magnitude of this change was small (Fig. 5*b*, Table 2). However, compared with EPSP onset latency, EPSP peak times varied greatly with sound location (EPSP peak latency$_{\text{contralateral}}$ of 26.9 ± 1.2 ms, EPSP peak latency$_{\text{ipsilateral}}$ of 35.5 ± 1.7 ms, $p < 0.001$, Friedman's test, $n = 22$) (Fig. 5*c*, Table 2). Thus, for contralateral sound locations, evoked EPSPs arrive at the soma more rapidly than those evoked by ipsilateral sound sources. This temporal organization of evoked synaptic potentials appears to reflect a fundamental property of acoustic spatial information arriving in auditory cortical pyramidal cells.

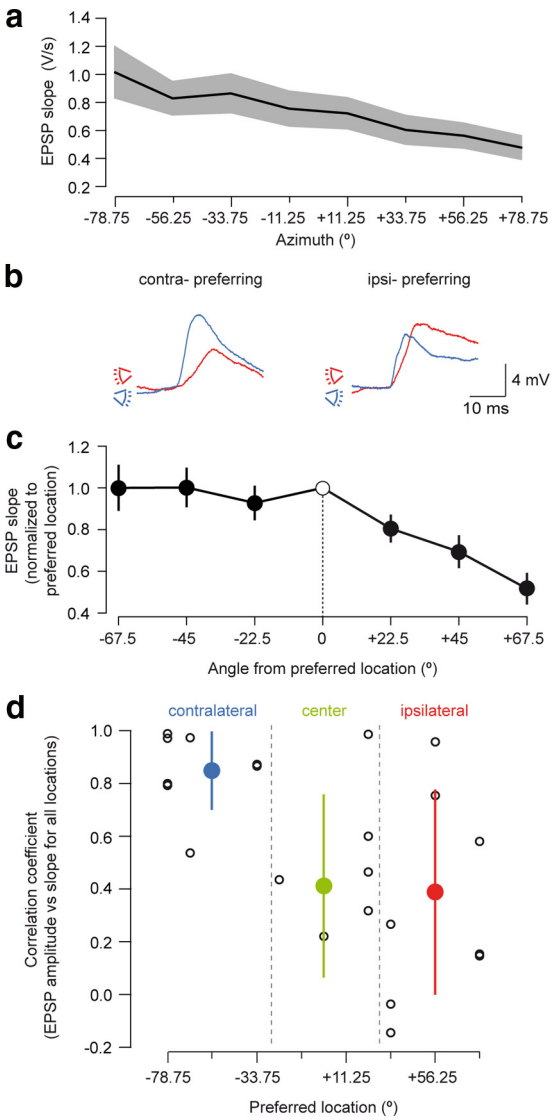

Figure 4. EPSP rising slope reflects sound source location. ***a***, Pooled average (black line) and SEM (gray area) of EPSP rising slope (10–90%, $n = 22$ cells). ***b***, Example averaged EPSP waveforms for contralateral-preferring (left) and ipsilateral-preferring (right) cells. Responses to contralateral sounds shown in blue, and ipsilateral sounds are shown in red. ***c***, Change in EPSP slope with angular deviation from preferred location. Contralateral deviations did not reduce EPSP slope, whereas ipsilateral deviations were associated with a significant decline (*$p < 0.01$, paired *t* test, $n = 22$). ***d***, Preferred location versus EPSP amplitude/rising slope correlation coefficient (mean ± SD; solid).

We have shown already that the preferred location of a given cell (i.e., the location evoking the largest synaptic response) is the site that most reliably evokes APs (Figs. 1*c*, 2*b*). Given the asymmetry in the distribution of EPSP rising slopes and that preferred location does not predict EPSP rates of rise, we next examined how the temporal properties of evoked responses relate to the SRF by quantifying the latency and reliability of AP firing with respect to sound location. Spike latency has been shown previously to vary with azimuth, the shortest latencies typically evoked by contralateral sounds (Brugge et al., 1996; Eggermont, 1998; Middlebrooks et al., 1998; Furukawa and Middlebrooks, 2002; Mickey and Middlebrooks, 2003; Stecker et al., 2003; Mrsic-Flogel et al., 2005). We observed a broad distribution in the mean

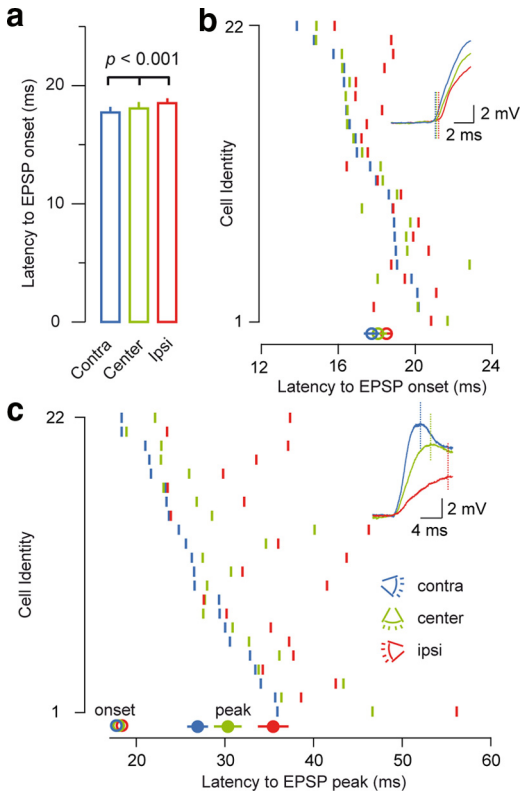

Figure 5. Precession of EPSP peak times across the horizontal plane. ***a***, EPSP onset latency (measured at 5% of EPSP peak) for contralateral, central, and ipsilateral sounds. Friedman's test was used to calculate significance. ***b***, Raster plot of latencies to EPSP onset for contralateral (blue), central (green), and ipsilateral (red) sounds. Inset, Onset latency for evoked contralateral, ipsilateral, and central EPSP waveforms for an example cell. ***c***, Raster plot of latencies to EPSP peak for contralateral (blue), central (green), and ipsilateral (red) sounds. Inset, Peak latency measurement of evoked contralateral, ipsilateral, and central EPSP waveforms for an example cell. Onset latencies are shown for comparison (open circles).

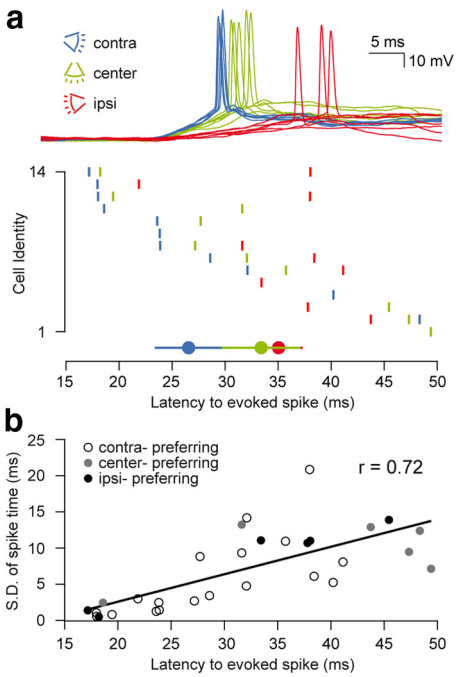

Figure 6. Latency and variability of spike timing is reduced for contralateral sound sources. ***a***, Top, Traces from a contralateral-preferring cell showing spiking to three locations (6 trials representative of the overall spike probability for the 3 locations, overlaid). Bottom, Raster plot of spike latency for cells that showed a minimum of four evoked spikes for at least one of contralateral (−78.25°; blue), central (0°; green), and ipsilateral (+78.25°; red) sound locations. ***b***, Relationship between mean spike latency and SD (white, gray, and black dots indicate contralateral-, central-, and ipsilateral-preferring neurons, respectively).

spike latency both within and across location (range for contralateral sounds: 17.2 to 48.3 ms, $n = 11$ cells in which contralateral locations evoked APs) (Fig. 6*a*), but spike latency was significantly shorter for contralateral than for ipsilateral sound sources ($p < 0.05$, Mann–Whitney U test) (Fig. 6*a*, Table 2). Furthermore, a clear relationship was observed between spike latency and precision (measured as the SD of spike latency; $r = 0.72$, $p < 0.01$, Spearman's rank correlation coefficient) (Fig. 6*b*, Table 2) regardless of preferred location. Because the SD of spike timing increased approximately linearly with respect to the mean latency (Phillips et al., 1989; Phillips and Hall, 1990; Heil, 1997), contralateral sound locations evoked spikes that were both earlier and more precise.

Thus, although the synaptic SRF does predict the location preference for spiking, it does not predict spike timing and reliability. At the population level, the relatively small decrease in EPSP amplitude across azimuth is also apparent in the change in spike probability (Fig. 7, black lines; Table 2). The change in EPSP rising slope is more marked, decreasing progressively in the ipsilateral direction. Consequently, and in contrast to spike probability, the speed and reliability of evoked spiking exhibit greater proportional decreases across the contralateral–ipsilateral axis (Fig. 7, red/gray lines). Together, these data indicate that, although sound source information is inherent in both the probability and the timing of spiking, these two parameters independently report different features of spatially tuned synaptic input.

Discussion

We have investigated how the profile of synaptic input arriving onto auditory cortical pyramidal cells influences spike probability and reliability during the representation of sound source location. Sound localization depends mostly on the extraction of binaural differences in the timing and level of sound between the two ears. In mammals, interaural time and level differences are computed by neurons of the auditory brainstem (Masterton et al., 1967; Boudreau and Tsuchitani, 1968; Goldberg and Brown, 1969; Tsuchitani and Boudreau, 1969; Yin and Chan, 1990) and, in concert with the monaural cues of absolute sound level and spectral composition, present the neocortex with information necessary for the representation of sound location (McAlpine, 2005). By varying sound location in the free field, these experiments incorporate the contribution of all naturally occurring spatial cues involved in sound localization. The evoked EPSPs recorded in this study are likely to result from a combination of direct thalamic and intracortical inputs (Kaur et al., 2004; Barbour and Callaway, 2008) and reflect a mixture of monaural and binaural spatial cues. Sound location modulated both the amplitude and timing of synaptic inputs, and, regardless of preferred location, we observed a precession of EPSP rise and peak times across the horizontal plane. This temporal sequence of synaptic input was reflected in the output of pyramidal cells, resulting in more rapid and reliably timed spiking in response to contralateral versus ipsilateral sounds.

Panoramic synaptic SRFs underlie spatially tuned pyramidal cell output

In agreement with previous studies, we found auditory stimulation to evoke sparse AP firing (DeWeese et al., 2003;

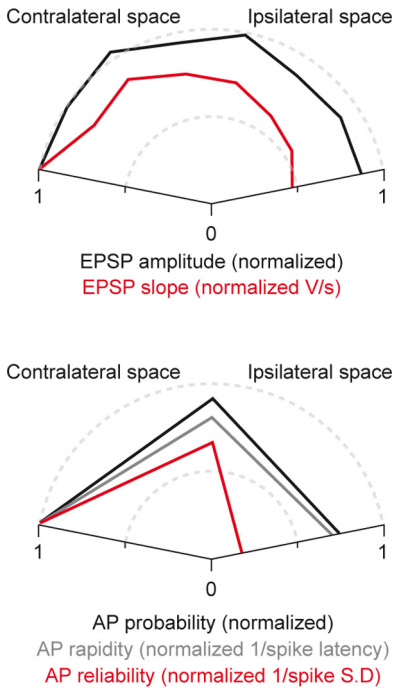

Figure 7. Distinct representations of auditory space via amplitude and timing in auditory cortex. Top, Mean change in EPSP amplitude (black) and slope (red) across the horizontal axis. Plot derived from eight locations, normalized to amplitude/slope at the most contralateral location tested (−78.75°). Bottom, Mean change in spike probability (black), rapidity (1/spike latency; gray), and reliability (1/SD of spike latency; red) across the horizontal axis. Plot was derived from three locations, normalized to probability/rapidity/reliability at the most contralateral location tested (−78.75°).

Stecker et al., 2003; Ulanovsky et al., 2004; Hromádka et al., 2008). Spiking SRFs were sharper and more narrowly tuned than their subthreshold counterparts, consistent with similar comparisons in other cortical sensory modalities (Zhu and Connors, 1999; Carandini and Ferster, 2000; Volgushev et al., 2000; Margrie et al., 2002). Spiking SRFs in this study were generally narrower than reported previously (Brugge et al., 1996; Mickey and Middlebrooks, 2003; Mrsic-Flogel et al., 2005; Stecker et al., 2005), and a large fraction (24 of 38) of neurons exhibited solely subthreshold responses. Unlike previous studies, our recordings were restricted to superficial layers of auditory cortex. One possibility is that spiking SRFs in superficial layers are narrower than in deeper layers and that acoustic space is more sparsely represented in superficial pyramidal cells. The narrowness of spectral receptive fields in A1 shows a similar laminar organization (Wallace and Palmer, 2008), as do receptive fields in other primary sensory cortical areas (Hubel and Wiesel, 1962; Martinez et al., 2005; de Kock et al., 2007). In addition, unlike conventional extracellular recordings, whole-cell recordings sample cells independent of their firing rate (Margrie et al., 2002, Hromádka et al., 2008). Cells with high firing rates previously recorded using extracellular techniques may also consequently exhibit broader spiking SRFs.

Regardless of the shape of its spiking SRF, every cell receives a panoramic view of acoustic space, such that a broadband sound from any location will generate a depolarization of membrane potential. Spatial tuning of auditory cortical pyramidal cells is therefore subject to a powerful "iceberg effect," whereby tuning is significantly broader below threshold than above it (Carandini and Ferster, 2000). Consequently, layer 2–4 pyramidal cells serve to refine and sharpen spatial information in a similar manner to spectral information (Wehr and Zador, 2003; Kaur et al., 2004; Liu et al., 2007). For such sharpening to occur, EPSP amplitude must be delicately balanced with respect to AP threshold, although cortical inhibition may also serve to limit the transformation of EPSP to spike (Wehr and Zador, 2003, Oswald et al., 2006; Wu et al., 2008).

Non-uniform subthreshold representations of acoustic space

Despite receiving synaptic input from across azimuth, the majority of cells exhibited preferred locations within contralateral space. This is in accordance with our spiking data and findings reported in previous studies (Middlebrooks and Pettigrew, 1981; Wise and Irvine, 1985; Imig et al., 1990; Rajan et al., 1990a; Middlebrooks and Green, 1991; Brugge et al., 1996; Stecker and Middlebrooks, 2003; Mrsic-Flogel et al., 2005; Stecker et al., 2005). However, a significant fraction of neurons received their strongest synaptic inputs in response to sounds at ipsilateral locations, the profile of ipsilateral-preferring SRFs effectively mirroring those of contralateral cells. Thus, within each hemisphere, there exists a complete but non-uniform representation of horizontal acoustic space distributed among the neuronal population.

EPSP rising slope decreases along the horizontal axis regardless of preferred location

We observed a functional separation between the spatial tuning of EPSP amplitude and kinetics: the EPSP rising slope (and consequently, the time of EPSP peak) was generally insensitive to preferred location, regardless of subthreshold tuning, and contralateral sounds evoked synaptic responses that reached their peak earlier than those evoked by ipsilateral sounds. Sound location information is therefore inherent in both the amplitude and rise time of synaptic activity.

For contralateral sounds, synaptic potentials had a steeper depolarization and evoked more precise spiking (Fetz and Gustafsson, 1983). Several mechanisms can potentially account for this variation in the temporal profile of synaptic depolarization with sound location. The small size of unitary thalamocortical EPSPs measured *in vivo* (Bruno and Sakmann, 2006) suggests that differences in EPSP slope observed here will likely arise from the integration of many individual inputs. As observed in vestibular-encoding synapses in the cerebellum (Arenz et al., 2008), sound source information in auditory cortex may be encoded via the frequency of synaptic input to pyramidal cells such that upstream spiking occurs within a narrower time window when evoked by contralateral sources. An alternative possibility is a relationship between spatial location of sound sources and the dendritic location of synapses encoding that information. The differences in the rise times of synaptic input evoked by contralateral versus ipsilateral sound sources observed here are consistent with differential attenuation of synaptic input arriving from proximal versus distal dendritic locations (Rall, 1962; Spruston et al., 1994; Magee, 2000). This scenario would require inputs encoding contralateral sounds to be located more proximal to the soma so that more distal ipsilateral inputs would be relatively more filtered in the dendrites. However, the considerable subcortical convergence of contralateral and ipsilateral input (e.g., in the lateral superior olive, inferior colliculus, and vMGB) (Delgutte et al., 1999; Samson et al., 2000; Tollin and Yin, 2002) suggests that, under such a scheme, local cortical connectivity would need to be highly organized across the entire somatodendritic axis.

Independent modulation of spike timing and probability by sound location

Spatially tuned synaptic inputs determine both the likelihood and the timing of action potential firing. We found that contralateral sounds evoked spikes with the shortest latencies, regardless of the preferred location of a cell. Therefore, preferred location predicts only the likelihood of a spike occurring: ipsilateral sounds will still generally evoke spikes later than contralateral sounds. Our data support the notion that the first-spike latency of a given neuron relative to population onset (Margrie and Schaefer, 2003) may be highly informative about sound source location (Heil, 2004; Chase and Young, 2007) and that there is a temporal representation of auditory space at the level of A1 (Eggermont, 1998; Eggermont and Mossop, 1998; Stecker and Middlebrooks, 2003). In addition, variability of spike timing is itself strongly correlated with first-spike latency (Phillips et al., 1989; Phillips and Hall, 1990; Heil, 1997), such that spike jitter is minimized for short-latency spikes (Schaefer et al., 2006). The precise timing of short-latency spikes may be in part attributable to rapidly evoked inhibition that is absent at later epochs (Tan et al., 2004; Wehr and Zador, 2005). However, we note that the timing of spikes evoked by slow-rising EPSPs is less reliable because spike generation is itself sensitive to the rate of membrane potential depolarization (Schaefer et al., 2006). This is, at least in part, attributable to an increase in the level of Na^+ channel inactivation during slow depolarizations (Hodgkin and Huxley, 1952; Azouz and Gray 1999). As such, the profile of the evoked excitatory synaptic input may itself be sufficient to account for the variability in spike timing.

As a consequence of fast-rising EPSPs and reduced AP jitter, contralaterally evoked spiking is likely to be more synchronously timed across the population, promoting rapid synaptic convergence at the downstream targets of pyramidal cells. Indeed, such a scheme may further exaggerate the difference between contralaterally and ipsilaterally evoked EPSP rising slopes at subsequent stages of auditory cortical processing. Sounds emanating from contralateral acoustic space will therefore be processed faster and more reliably than those from ipsilateral space, favoring accurate spatial localization and discrimination of the opposite hemifield (Stecker et al., 2005; Miller and Recanzone, 2009).

Finally, although synaptic inputs to auditory cortex provide a panoramic representation of acoustic space that is reflected in spike output in the strongest regions of the SRF, the independent influence of sound location on the temporal profile of synaptic and spiking activity suggests that spatial representation is unlikely to depend solely on an identity code based on preferred location. Information regarding sound location is conveyed in both the strength and kinetics of synaptic depolarization. A surfeit of contralaterally tuned neurons and a fixed temporal precession of EPSP rise times across the horizontal axis favor accurate contralateral representations of acoustic space in auditory cortical output.

References

Arenz A, Silver RA, Schaefer AT, Margrie TW (2008) The contribution of single synapses to sensory representation *in vivo*. Science 321:977–980.

Azouz R, Gray CM (1999) Cellular mechanisms contributing to response variability of cortical neurons *in vivo*. J Neurosci 19:2209–2223.

Barbour DL, Callaway EM (2008) Excitatory local connections of superficial neurons in rat auditory cortex. J Neurosci 28:11174–11185.

Boudreau JC, Tsuchitani C (1968) Binaural interaction in the cat superior olive S segment. J Neurophysiol 31:442–454.

Brugge JF, Reale RA, Hind JE (1996) The structure of spatial receptive fields of neurons in primary auditory cortex of the cat. J Neurosci 16:4420–4437.

Bruno RM, Sakmann B (2006) Cortex is driven by weak but synchronously active thalamocortical synapses. Science 312:1622–1627.

Carandini M, Ferster D (2000) Membrane potential and firing rate in cat primary visual cortex. J Neurosci 20:470–484.

Chase SM, Young ED (2007) First-spike latency information in single neurons increases when referenced to population onset. Proc Natl Acad Sci U S A 104:5175–5180.

Cruikshank SJ, Rose HJ, Metherate R (2002) Auditory thalamocortical synaptic transmission *in vitro*. J Neurophysiol 87:361–384.

de Kock CP, Bruno RM, Spors H, Sakmann B (2007) Layer- and cell-type specific suprathreshold stimulus representation in rat primary somatosensory cortex. J Physiol 581:139–154.

Delgutte B, Joris PX, Litovsky RY, Yin TC (1999) Receptive fields and binaural interactions for virtual-space stimuli in the cat inferior colliculus. J Neurophysiol 81:2833–2851.

DeWeese MR, Wehr M, Zador AM (2003) Binary spiking in auditory cortex. J Neurosci 23:7940–7949.

Eggermont JJ (1998) Azimuth coding in primary auditory cortex of the cat. II. Relative latency and interspike interval representation. J Neurophysiol 80:2151–2161.

Eggermont JJ, Mossop JE (1998) Azimuth coding in primary auditory cortex of the cat. I. Spike synchrony versus spike count representations. J Neurophysiol 80:2133–2150.

Fetz EE, Gustafsson B (1983) Relation between shapes of post-synaptic potentials and changes in firing probability of cat motoneurones. J Physiol 341:387–410.

Furukawa S, Middlebrooks JC (2002) Cortical representation of auditory space: information-bearing features of spike patterns. J Neurophysiol 87:1749–1762.

Goldberg JM, Brown PB (1969) Response of binaural neurons of dog superior olivary complex to dichotic tonal stimuli: some physiological mechanisms of sound localization. J Neurophysiol 32:613–636.

Heffner HE, Heffner RS (1990) Effect of bilateral auditory cortex lesions on sound localization in Japanese macaques. J Neurophysiol 64:915–931.

Heffner H, Masterton B (1975) Contribution of auditory cortex to sound localization in the monkey (*Macaca mulatta*). J Neurophysiol 38:1340–1358.

Heil P (1997) Auditory cortical onset responses revisited. I. First-spike timing. J Neurophysiol 77:2616–2641.

Heil P (2004) First-spike latency of auditory neurons revisited. Curr Opin Neurobiol 14:461–467.

Hodgkin AL, Huxley AF (1952) The dual effect of membrane potential on sodium conductance in the giant axon of Loligo. J Physiol 116:497–506.

Horikawa K, Armstrong WE (1988) A versatile means of intracellular labelling: injection of biocytin and its detection with avidin conjugates. J Neurosci Methods 25:1–11.

Hromádka T, Deweese MR, Zador AM (2008) Sparse representation of sounds in the unanesthetized auditory cortex. PLoS Biol 6:e16.

Hubel DH, Wiesel TN (1962) Receptive fields, binocular interaction and functional architecture in the cat's visual cortex. J Physiol 160:106–154.

Imig TJ, Irons WA, Samson FR (1990) Single-unit selectivity to azimuthal direction and sound pressure level of noise bursts in cat high-frequency primary auditory cortex. J Neurophysiol 63:1448–1466.

Jenkins WM, Masterton RB (1982) Sound localization: effects of unilateral lesions in central auditory system. J Neurophysiol 47:987–1016.

Jenkins WM, Merzenich MM (1984) Role of cat primary auditory cortex for sound-localization behavior. J Neurophysiol 52:819–847.

Kalatsky VA, Polley DB, Merzenich MM, Schreiner CE, Stryker MP (2005) Fine functional organization of auditory cortex revealed by Fourier optical imaging. Proc Natl Acad Sci U S A 102:13325–13330.

Kaur S, Lazar R, Metherate R (2004) Intracortical pathways determine breadth of subthreshold frequency receptive fields in primary auditory cortex. J Neurophysiol 91:2551–2567.

Kavanagh GL, Kelly JB (1987) Contribution of auditory cortex to sound localization by the ferret (*Mustela putorius*). J Neurophysiol 57:1746–1766.

Liu BH, Wu GK, Arbuckle R, Tao HW, Zhang LI (2007) Defining cortical frequency tuning with recurrent excitatory circuitry. Nat Neurosci 10:1594–1600.

Magee JC (2000) Dendritic integration of excitatory synaptic input. Nat Rev Neurosci 1:181–190.

Malhotra S, Lomber SG (2007) Sound localization during homotopic and heterotopic bilateral cooling deactivation of primary and nonprimary auditory cortical areas in the cat. J Neurophysiol 97:26–43.
Margrie TW, Schaefer AT (2003) Theta oscillation coupled spike latencies yield computational vigour in a mammalian sensory system. J Physiol 546:363–374.
Margrie TW, Brecht M, Sakmann B (2002) In vivo, low-resistance, whole-cell recordings from neurons in the anaesthetized and awake mammalian brain. Pflügers Arch 444:491–498.
Margrie TW, Meyer AH, Caputi A, Monyer H, Hasan MT, Schaefer AT, Denk W, Brecht M (2003) Targeted whole-cell recordings in the mammalian brain *in vivo*. Neuron 39:911–918.
Martinez LM, Wang Q, Reid RC, Pillai C, Alonso JM, Sommer FT, Hirsch JA (2005) Receptive field structure varies with layer in the primary visual cortex. Nat Neurosci 8:372–379.
Masterton B, Jane JA, Diamond IT (1967) Role of brainstem auditory structures in sound localization. I. Trapezoid body, superior olive, and lateral lemniscus. J Neurophysiol 30:341–359.
McAlpine D (2005) Creating a sense of auditory space. J Physiol 566:21–28.
Mickey BJ, Middlebrooks JC (2003) Representation of auditory space by cortical neurons in awake cats. J Neurosci 23:8649–8663.
Middlebrooks JC, Green DM (1991) Sound localization by human listeners. Annu Rev Psychol 42:135–159.
Middlebrooks JC, Pettigrew JD (1981) Functional classes of neurons in primary auditory cortex of the cat distinguished by sensitivity to sound location. J Neurosci 1:107–120.
Middlebrooks JC, Xu L, Eddins AC, Green DM (1998) Codes for sound source location in nontonotopic auditory cortex. J Neurophysiol 80: 863–881.
Miller LM, Recanzone GH (2009) Populations of auditory cortical neurons can accurately encode acoustic space across stimulus intensity. Proc Natl Acad Sci U S A 106:5931–5935.
Mrsic-Flogel TD, King AJ, Schnupp JW (2005) Encoding of virtual acoustic space stimuli by neurons in ferret primary auditory cortex. J Neurophysiol 93:3489–3503.
Oswald AM, Schiff ML, Reyes AD (2006) Synaptic mechanisms underlying auditory processing. Curr Opin Neurobiol 16:371–376.
Paxinos G, Watson C (2004) The rat brain in stereotaxic coordinates: the new coronal set, Ed 5. New York: Academic.
Phillips DP, Hall SE (1990) Response timing constraints on the cortical representation of sound time structure. J Acoust Soc Am 88:1403–1411.
Phillips DP, Hall SE, Hollett JL (1989) Repetition rate and signal level effects on neuronal responses to brief tone pulses in cat auditory cortex. J Acoust Soc Am 85:2537–2549.
Polley DB, Read HL, Storace DA, Merzenich MM (2007) Multiparametric auditory receptive field organization across five cortical fields in the albino rat. J Neurophysiol 97:3621–3638.
Rajan R, Aitkin LM, Irvine DR, McKay J (1990a) Azimuthal sensitivity of neurons in primary auditory cortex of cats. I. Types of sensitivity and the effects of variations in stimulus parameters. J Neurophysiol 64:872–887.
Rajan R, Aitkin LM, Irvine DR (1990b) Azimuthal sensitivity of neurons in primary auditory cortex of cats. II. Organization along frequency-band strips. J Neurophysiol 64:888–902.
Rall W (1962) Theory of physiological properties of dendrites. Ann NY Acad Sci 96:1071–1092.
Read HL, Winer JA, Schreiner CE (2002) Functional architecture of auditory cortex. Curr Opin Neurobiol 12:433–440.
Rutkowski RG, Miasnikov AA, Weinberger NM (2003) Characterisation of multiple physiological fields within the anatomical core of the rat auditory cortex. Hear Res 181:116–130.
Samson FK, Barone P, Irons WA, Clarey JC, Poirier P, Imig TJ (2000) Directionality derived from differential sensitivity to monaural and binaural cues in the cat's medial geniculate body. J Neurophysiol 84:1330–1345.
Schaefer AT, Angelo K, Spors H, Margrie TW (2006) Neuronal oscillations enhance stimulus discrimination by ensuring action potential precision. PLoS Biol 4:e163.
Spruston N, Jaffe DB, Johnston D (1994) Dendritic attenuation of synaptic potentials and currents: the role of passive membrane properties. Trends Neurosci 17:161–166.
Stecker GC, Mickey BJ, Macpherson EA, Middlebrooks JC (2003) Spatial sensitivity in field PAF of cat auditory cortex. J Neurophysiol 89:2889–2903.
Stecker GC, Middlebrooks JC (2003) Distributed coding of sound locations in the auditory cortex. Biol Cybern 89:341–349.
Stecker GC, Harrington IA, Middlebrooks JC (2005) Location coding by opponent neural populations in the auditory cortex. PLoS Biol 3:e78.
Tan AY, Zhang LI, Merzenich MM, Schreiner CE (2004) Tone-evoked excitatory and inhibitory synaptic conductances of primary auditory cortex neurons. J Neurophysiol 92:630–643.
Thompson GC, Cortez AM (1983) The inability of squirrel monkeys to localize sound after unilateral ablation of auditory cortex. Behav Brain Res 8:211–216.
Tollin DJ, Yin TC (2002) The coding of spatial location by single units in the lateral superior olive of the cat. I. Spatial receptive fields in azimuth. J Neurosci 22:1454–1467.
Tsuchitani C, Boudreau JC (1969) Stimulus level of dichotically presented tones and cat superior olive S-segment cell discharge. J Acoust Soc Am 46:979–988.
Ulanovsky N, Las L, Farkas D, Nelken I (2004) Multiple time scales of adaptation in auditory cortex neurons. J Neurosci 24:10440–10453.
Volgushev M, Pernberg J, Eysel UT (2000) Comparison of the selectivity of postsynaptic potentials and spike responses in cat visual cortex. Eur J Neurosci 12:257–263.
Wallace MN, Palmer AR (2008) Laminar differences in the response properties of cells in the primary auditory cortex. Exp Brain Res 184:179–191.
Wehr M, Zador AM (2003) Balanced inhibition underlies tuning and sharpens spike timing in auditory cortex. Nature 426:442–446.
Wehr M, Zador AM (2005) Synaptic mechanisms of forward suppression in rat auditory cortex. Neuron 47:437–445.
Werner-Reiss U, Groh JM (2008) A rate code for sound azimuth in monkey auditory cortex: implications for human neuroimaging studies. J Neurosci 28:3747–3758.
Winer JA (1992) The mammalian auditory pathway: neuroanatomy, Vol 1 (Popper AN, Fay RR, Webster DB, eds), pp 222–409. New York: Springer.
Wise LZ, Irvine DR (1985) Topographic organization of interaural intensity difference sensitivity in deep layers of cat superior colliculus: implications for auditory spatial representation. J Neurophysiol 54:185–211.
Wu GK, Arbuckle R, Liu BH, Tao HW, Zhang LI (2008) Lateral sharpening of cortical frequency tuning by approximately balanced inhibition. Neuron 58:132–143.
Yin TC, Chan JC (1990) Interaural time sensitivity in medial superior olive of cat. J Neurophysiol 64:465–488.
Zhou B, Green DM, Middlebrooks JC (1992) Characterization of external ear impulse responses using Golay codes. J Acoust Soc Am 92:1169–1171.
Zhu JJ, Connors BW (1999) Intrinsic firing patterns and whisker-evoked synaptic responses of neurons in the rat barrel cortex. J Neurophysiol 81:1171–1183.